

Deformations in wide, center-notched, thin panels, part I: three-dimensional shape and deformation measurements by computer vision

Jeffrey D. Helm, MEMBER SPIE
Lafayette College
Department of Mechanical Engineering
Easton, Pennsylvania 18042

Michael A. Sutton
Stephen R. McNeill
University of South Carolina
Department of Mechanical Engineering
Columbia, South Carolina 29208

Abstract. The response of wide, thin, center-notched, 2024-T3 aluminum panels undergoing far-field tensile load is investigated. Three panels with a notch length to panel width of 0.33 and widths of 305, 610, and 1016 mm were subjected to far-field tensile loading. As part of the experimental program, two pairs of cameras were configured into separate stereovision systems and used to simultaneously capture both the global response of the sheet and the local response near a notch tip. Global areas, ranging in size from 250×250 mm to 550×550 mm, were imaged for each panel. A second stereovision system recorded images of a small area, 10×20 mm, ahead of one notch tip. Postprocessing of the stereovision measurement data from global and local systems using three-dimensional digital image correlation was used to obtain the complete displacement field at each point in the region of interest. In general, results demonstrate that the combination of stereovision and three-dimensional digital image correlation is capable of accurately measuring true, three-dimensional structural deformations in regions undergoing both large out-of-plane displacements and large displacement gradients. Furthermore, 3-D measurements on the panel specimen near the grip location are shown to provide an independent assessment of the true boundary conditions, with specimen slippage clearly noted in the 1016-mm specimen. Results from the extensive notched, wide panel experimental program demonstrate that (a) each panel has an initial shape that deviates up to 3 mm from planarity, with the greatest deviations occurring at the center of the notch, (b) the global load-displacement response is essentially linear for load levels that are well beyond the onset of large, out-of-plane displacements in the notch region, and (c) increasing the size of the notched, thin panel specimen results in distinctly different surface deformations and deformed shapes, with three separate maxima/minima in the out-of-plane component of the largest panel. The region where tensile opening strains are above 2% extends several millimeters ahead of the hole, while compressive strains parallel to the notch direction are contained within a few millimeters of the hole. The in-plane shear strains are concentrated along circular lobes at ± 45 deg from the horizontal direction, a trend which is generally consistent with plane stress conditions. © 2003 Society of Photo-Optical Instrumentation Engineers.

[DOI: 10.1117/1.1566001]

Subject terms: center-notched wide aluminum panels; tensile loading; stereovision systems; 3-D digital image correlation; full-field displacement and strain measurements.

Paper MET-01 received Aug. 17, 2002; revised manuscript received Nov. 15, 2002; accepted for publication Nov. 15, 2002.

1 Introduction

In the early 1990s, the United States launched a national research program directed toward identifying and understanding the fundamental issues in the aging of our aerospace systems. National agencies such as the National Aeronautics and Space Administration (NASA), the Federal Aviation Administration (FAA), and the United States Air Force (USAF) were directed to assist in the overall

effort. NASA Langley, Wright Patterson Air Force Base (WPAFB), and the newly formed FAA Research Center staffed and operated research programs to develop both the experimental and analytical tools necessary for characterizing and predicting how aging affects the response of aerospace structures.

Over the past decade, a wide range of experimental methods have been developed to monitor aerospace struc-

tures. Examples of the technologies that have been developed in the past decade include eddy-current probes and ultrasonic devices to identify small flaws near rivet holes, thermography systems to identify areas of debonding in lap joints, and shape measurement systems to identify structural bulges in regions of extensive corrosion. Though these areas continue to be important for nondestructive evaluation of structures, none of these methods are capable of providing quantitative, full-field three-dimensional deformation data for large structural components undergoing loading; such information is essential to the development and validation of computational model predictions, especially when flaws and/or geometric imperfections are present.

As part of the overall effort, investigators at NASA Langley focused on the development and validation of computational methodologies for predicting residual strength in large aerospace structures. To some extent, this was due to the work of Forman.¹ Dr. Forman performed a series of tests in 1966 on wide, thin, middle-crack tension [M(T)] specimens. His work clearly showed that tensile loading of the M(T) panels resulted in significant out-of-plane deformations at the center of the panel, accompanied by a 25% reduction in residual strength relative to a test where out-of-plane motion was restrained.

Reliable and useful computational models for use in full-scale aerospace applications were quickly developed [e.g., Structural analysis of general shells (STAGS),² WARP3D³]. Initial modeling of the response of a group of constrained panels proved quite promising. Seshadri et al.⁴ demonstrated the ability of the STAGS finite element code to predict the measured load-crack extension response of constrained 1016-mm-wide, center-cracked panels (when buckling was prevented). However, when the same analysis was performed for unconstrained panels, the difference between the finite element predictions and experimental results nearly doubled.

Because behavior similar to that observed by Foreman has been shown to be present during the failure of airframe components,⁵ resulting in complex crack tip conditions for unconstrained fracture surfaces,^{4,6} both experimental measurements (Part I) and computational studies (Part II) of the unconstrained response of M(T) panels prior to crack growth have been performed. In Part I, the emphasis is on full-field, 3-D deformation measurements in thin, wide, notched panels. Notches are used so that the experimental results can be directly compared to computational model predictions prior to observable crack initiation.

Since initial laboratory studies had been done to demonstrate the potential of computer vision systems⁷⁻⁹ the authors developed a robust, novel 3-D digital image correlation methodology¹⁰ capable of acquiring stereovision images and analyzing the images to determine the three-dimensional deformations in large panels while automatically including the effects of perspective distortion.^{11,12} The technique has been used for the characterization of crack growth in aluminum panels subjected to tension-torsion loadings,^{13,14} which have both large out-of-plane displacements and large in-plane strains. To better understand how far-field loadings affect local behavior, a global-local system was employed to simultaneously measure deformations in large areas and selected small areas near flaws or discon-

tinuities. The global-local system utilizes two separate stereovision systems, one measuring deformations for a large portion of the specimen and the second measuring deformations in a small area of interest. The combined system's capabilities have previously been demonstrated through successful measurement of the compressive response of notched composite panels.¹⁵

In the work presented here, we will report on the experimental investigations that have been completed for a series of tensile tests on wide, M(T), center notched tensile specimens. It is emphasized that notched panels were used to focus attention on the relationship between measurements and modeling predictions during large-scale deformations and displacements, but prior to the added complexities of stable crack growth. In Sec. 2, the wide panel geometry and loading process are described. In Sec. 3, the computer vision setup for acquiring three-dimensional measurements on both the global and local scale is described. In Sec. 4, the 3-D measurement process is discussed and the data transformation required for conversion to a specimen-based coordinate system is outlined. In Sec. 5, 3-D measurement results from all three panels are presented for (a) the initial surface shape, (b) full-field, global 3-D displacements, and (c) local surface strains. In Secs. 6 and 7, the experimental results are discussed and concluding remarks provided.

2 Wide Panel M(T) Geometry and Loading Process

Figure 1 presents a schematic of the middle-flawed tension specimen [M(T)] geometry used in this work. All of the wide panel test specimens were machined from 1.6-mm-thick, unclad 2024-T3 aluminum sheets. Three panel geometries, with $2w = 305, 610, \text{ and } 1016 \text{ mm}$; $2h = 610, 1270, \text{ and } 1570 \text{ mm}$; and a notch-length-to-specimen-width of $a/w = 0.33$ for all panels, were used in this experimental program. All specimens were machined in the LT orientation; the rolling direction of the material is perpendicular to the direction of the central notch. To eliminate stable crack growth, the central notch in the panel was terminated in a pair of 4.76-mm-diam holes; both holes and notch were machined into the panels by wire EDM.

All experiments were performed at the structural test facility in Building 1205 at the NASA Langley Research Center in Hampton, Virginia. Tension loading was applied to each specimen through large steel grips clamped to the ends of the specimen. Figure 2 shows the tensile grip details. The holes machined in the gripping region of the specimen were approximately 1.6 mm larger in diameter than the 27-mm bolts used to fasten the specimen into the tensile grips. In addition to oversized specimen holes, a thin piece of flexible plastic sheet, approximately 1 mm thick, was placed between the specimen surface and the grips to produce a more uniform clamping condition within the grips. The grip bolts were tightened in a predetermined alternating sequence, with an impact wrench used to complete the bolt-up process.

All tests were run under displacement control on either a 448-kN (305-mm panel) or a 1.3-MN (610- and 1016-mm panels) servo-hydraulic test frame. Figure 3 shows the 1.3-MN, four-post, tension loading frame and a 1016-mm-wide M(T) specimen. The ramp rate for the applied grip displacement varied from 0.17 per min (305-mm panel) to

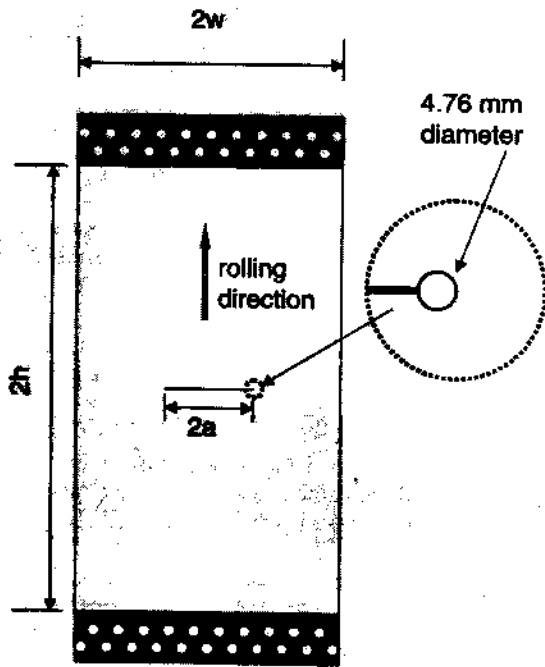


Fig. 1 Specimen geometry.

0.25 mm per min (610- and 1016-mm panels). At periodic intervals, the loading was interrupted to allow image data to be acquired. In addition to image data, load and displacement data from the test stand were monitored and recorded every five seconds throughout the loading process.

3 Stereovision Measurement Systems

In this section, details will be presented regarding (a) the arrangement of the global and local 3-D computer vision systems, (b) the 3-D vision model and calibration procedures, (c) the image correlation process for measuring 3-D surface deformations, and (d) specific issues that arose with the global measurements.

3.1 Experimental Arrangement of 3-D Systems

Since each panel required a different computer vision setup, Table 1 provides a summary of key experimental details for all panels in the experimental program. The global imaging

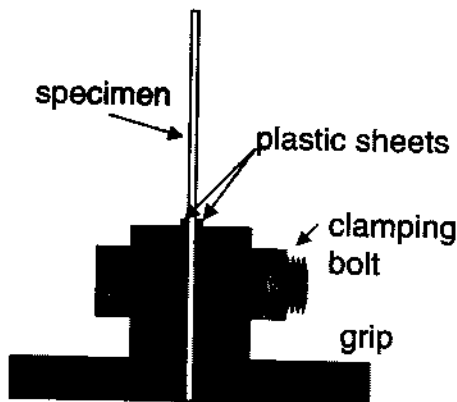


Fig. 2 Tensile grip detail.

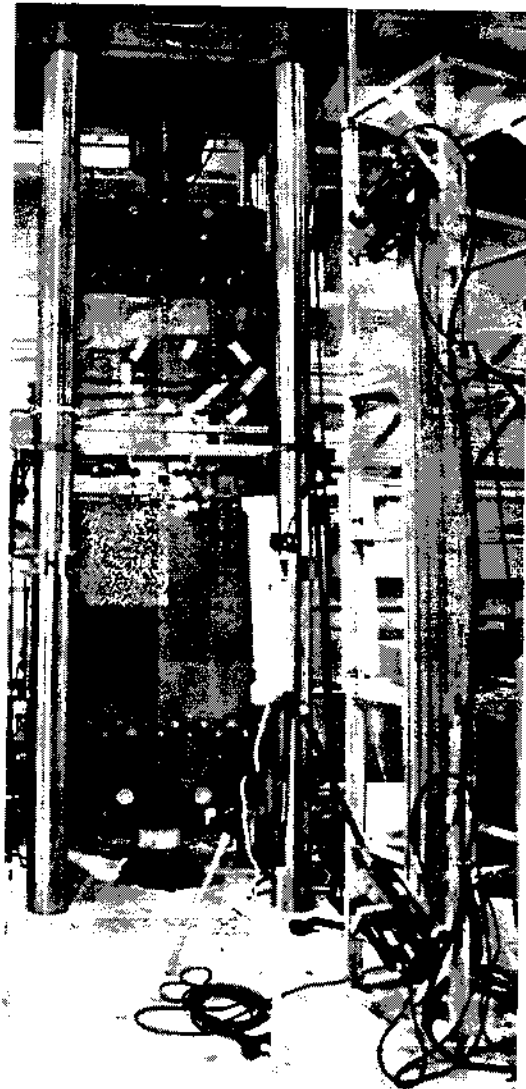


Fig. 3 Stereovision system for global image acquisition (visible on right side mounted vertically on frame) with 1.3-MN tension loading frame and 1016-mm panel specimen.

system, shown on the right side of Fig. 3, was stationary throughout the loading process. The local imaging system, shown in Fig. 4, was mounted on an additional translation stage so it could be moved to track the location of the hole at the end of the notch with images acquired both prior to loading and then at designated load levels.

As noted in Table 1, the cameras have direct analog-to-digital conversion within the camera, reducing system noise and eliminating uncertainty in the pixel location that is introduced when an analog camera signal is digitized in the computer. The local system uses a high-quality, 100-mm-focal-length Canon lens with 2X extenders to achieve the magnification required for the experiments.

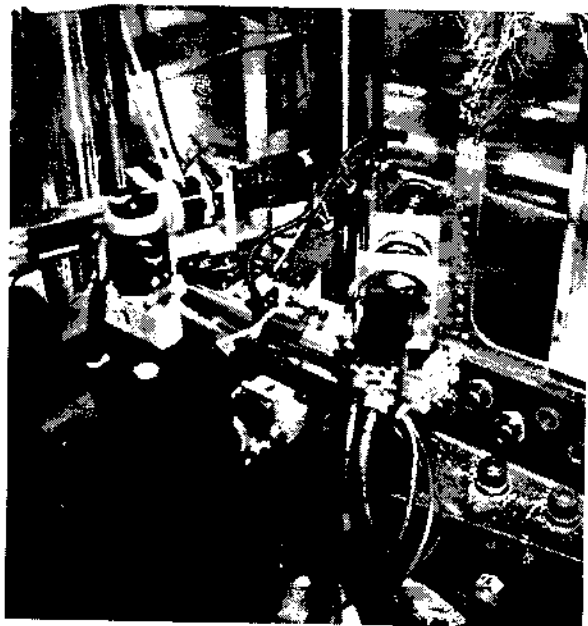
It is noted that the global imaging setup for the 610- and 1016-mm panel experiments was performed with the camera rotated 90 deg (see Fig. 3) and mounted vertically so that the maximum imaging resolution corresponded with the largest object distance to be imaged. Because the support columns of the 1.3-MN test machine interfered with the ability to view the surface of the panel with the cameras

Table 1 Summary of experimental stereovision measurement system specifications and error estimates.

	Global stereovision system			Local stereovision system		
	305-mm panel	610-mm panel	1016-mm panel	305-mm panel	610-mm panel	1016-mm panel
Random pattern application method	Self-adhesive white vinyl with random black pattern printed on vinyl			White acrylic paint background with light dusting of black acrylic paint		
Viewing area	330×380 mm (more than $\frac{1}{2}$ of specimen area)	650×700 mm (more than $\frac{1}{2}$ of specimen area)	300×400 mm (more than $\frac{1}{4}$ of specimen area)	23×15 mm	21×13 mm	20×12 mm
Camera type and resolution	Pulnix 9701 direct digital CCD; ratio of vertical to horizontal pixel dimensions is $\lambda = 0.8533$; imaging array has 768 pixels horizontal by 484 pixels vertical					
Lens types	Canon 28-mm lenses	Schneider 10-mm rectilinear lenses		Canon 100-mm macro lenses		
Camera separation and distance to specimen	1.2 m apart; 1.2 m from specimen	0.80 m apart; 1.2 m from specimen	0.60 m apart; 0.90 m from specimen	0.24 m apart; 0.35 m from specimen		0.28 m apart; 0.34 m from specimen
Camera pair orientation	Horizontal platform; Included pan angle ≈ 53 deg	Vertical platform; included pan angle ≈ 37 deg	Vertical platform; included pan angle ≈ 37 deg	Horizontal platform; included pan angle ≈ 38 deg		
Standard deviation for 3-D measurements	10 μm	60 μm	50 μm		1 μm	
Peak-to-peak variations in 3-D measurements	± 50 μm	± 200 μm	± 300 μm		± 10 μm	

system perpendicular to the panel, the entire camera system was rotated so the panel is viewed from ~ 10 deg off-axis, as shown in Fig. 3.

For calibration of the global and local measurement systems, each camera was mounted on a translation stage that provided movement along the optical axis. Each 3-D system had its own computer for controlling the cameras, acquiring and storing the image data, and controlling the movement of all translation stages.

**Fig. 4** Stereovision system for local image acquisition.

3.2 Imaging Model and Calibration Process

Because the background development for the use of stereovision systems in 3-D measurements has been presented in previous publications,^{7-12,16-18} only a brief overview of the imaging model and the camera calibration process will be presented.

As in previous work, the camera and lens system are modeled as a pinhole device with a correction term to account for lens distortion. The required parameters for this imaging model include five intrinsic parameters [e.g., pinhole distance (phd), image center (C_x, C_y), aspect ratio, λ , and a distortion coefficient, κ ^{9-11,17}] and six extrinsic parameters including the angular location variables (α, β, γ) and the position of the origin (X_o, Y_o, Z_o).

The calibration process determines the eleven parameters that describe the position and orientation of the cameras and their operating characteristics. To determine the eleven parameters noted above, there are several "calibration procedures" that have been developed. In this work, the calibration process is performed independently for each camera by imaging a series of images for a 10 by 10 calibration grid with known spacing. Following the procedures outlined by Helm,¹⁰ a grid is placed in the general vicinity where experimental data will be acquired and an initial image acquired by both cameras in a 3-D imaging system. Each camera is then moved perpendicular to its sensor plane and a second pair of images acquired.

Using the known spacing of the grid, the previously measured aspect ratio of the camera, the known movement of the camera, and the location of the grid intersections (as extracted from the calibration images), a nonlinear optimization process is used to obtain the ten remaining camera parameters that provide the best estimate for the known

grid spacing. Because the position of each camera is measured with respect to the same grid, the relative positions of the cameras are known after camera calibration is completed. It is worth noting that two different grids were used to calibrate the global and local camera systems, a large one with a grid spacing of 19.05 mm and a smaller one with a grid spacing of 0.5 mm, respectively.

4 Three-dimensional Measurement Process

Surface displacements are determined by correlating images acquired from each camera before and after deformation. By locating common areas in all images of the object using image correlation, and knowing the camera parameters, the system measures both the initial shape of the object (profiling) and the true, full-field, three-dimensional displacements of the object.

To perform the image correlation process for three-dimensional measurements, the surface is required to have a characteristic pattern visible to all stereovision system cameras. A random pattern is typically used for this purpose, as it is usually easy to create. Techniques to apply the pattern include photolithography,¹⁹ overspray of spray paint and/or spattering of paint,²⁰ direct xeroxing of pattern,^{21,22} sprinkling and melting to adhere toner powder onto surface,²³ and bonding of printed vinyl.¹⁵ The technique used is mostly dependent on the scale of the area to be measured. However, other measurement requirements (e.g., the specimen material) may affect the choice of pattern application procedure. This work used the printed vinyl for the far-field measurements and an overspray of black spray paint onto a white base coating of enamel spray paint for the local measurements.

The back-projection method developed by Helm et al.¹⁰ and shown schematically in Fig. 5 is used to locate the spatial position of a specific image subset. By assuming that a planar patch can describe a small object region, an initial 3-D position and orientation for the planar region are established through an interactive first-guess generator. Since the operating characteristics of each camera are known, the gray levels of a subset in camera 0 can be mathematically projected onto the candidate plane, creating a virtual gray-level pattern in space. The positions of the virtual gray-level pattern are then projected into camera 1, identifying a second gray-level pattern on the sensor plane. By optimizing the candidate plane parameters to minimize the nonlinear cross-correlation error function between the two gray-level patterns, the projection of the center of the subset onto the candidate plane describes the location in space of the center of the subset.

Since this process can be performed for the undeformed object and then repeated to locate the same regions after deformation, both the initial surface shape of the object and the 3-D displacements for all object points that are imaged in both cameras will be measured. The estimates for 3-D measurement errors given in Table 1 are based on both (a) the calibration procedure in Sec. 3.2 and (b) the back-projection process noted above.

Finally, it is noted that the components of the initial 3-D data obtained using image correlation are given in a coordinate system that is defined in a nonphysical system centered at the pinhole of camera 0. To compare the experimental results with finite element predictions, the image

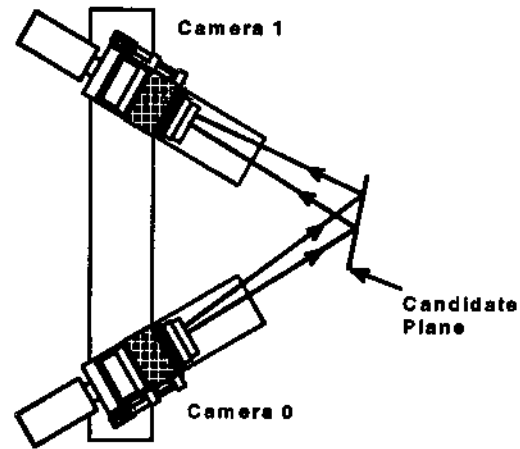


Fig. 5 Back-projection process for determining the 3-D location of a subset.

correlation data was transformed to a coordinate system with (a) the Z axis perpendicular to the plane that best describes the initial shape of the panel, (b) the X axis aligned with the horizontal line of data closest to the grip-panel interface, (c) the Y axis aligned with the vertical centerline of the panel, and (d) $X=0, Y=0$ location at the center of the panel. Thus, the X axis is in the direction of the notch, the Y axis is along the vertical centerline of the plate, and the Z axis is in the through-thickness direction for the panel. Positive X values are to the right side of the panel as viewed from the front, positive Y values are upward, and positive Z values indicate movement toward the camera system.

It is noted that the line of data near the grip location is used to define the X-axis since the sheet was rigidly clamped in this region and provided a well-defined horizontal reference line for future data comparisons.

5 Displacement and Shape Measurements

To obtain three-dimensional surface data, images were obtained with the global and local 3-D systems. All images were analyzed using software, designated VIC-3D, that incorporates the concepts outlined in Secs. 3.2 and 3.3 to

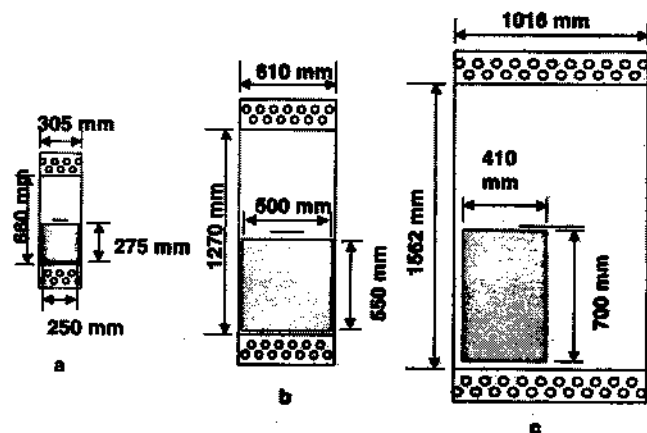


Fig. 6 3-D deformation measurement areas.

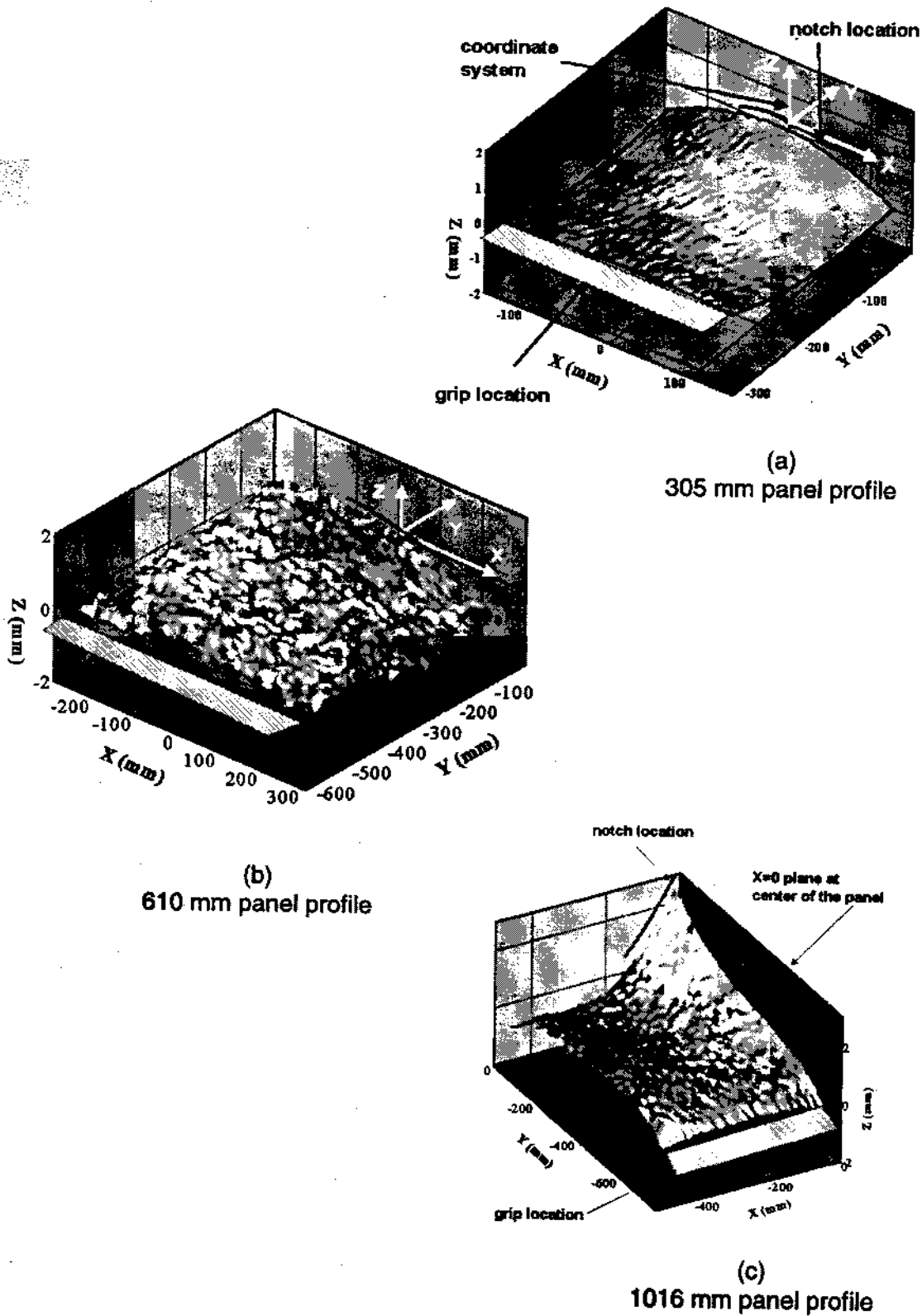


Fig. 7 Initial profiles for panels of widths 305, 610, and 1016 mm.

determine (a) the initial shape, (b) the full-field, three-dimensional surface displacements for large areas of the panels, and (c) selected lines of displacement data that were extracted from the global data fields for later comparison with finite element predictions.

Local 3-D measurements were obtained throughout the area indicated in Table 1, centered on the termination drill hole. As shown in Fig. 6, global 3-D measurements were obtained in slightly smaller areas than indicated in Table 1. Global surface displacements were measured at approxi-

mately 5,800 points from each pair of images using a subset size of 33×33 pixels. Local data was obtained at approximately 23,000 points also using a subset size of 33×33 pixels. Approximate in-plane magnification factors for each panel with the global measurement system were 0.36 mm/pixel (305-mm panel), 0.71 mm/pixel (610-mm panel), and 0.91 mm/pixel (1016-mm panel). The approximate in-plane magnification factor for all panels using the local measurement system was 0.025 mm/pixel.

Image analysis was performed on the image data for each panel for $P=0$, $P_{\max}/4$, $P_{\max}/2$, $3P_{\max}/4$, $7P_{\max}/8$, and P_{\max} , where P_{\max} is the load just before catastrophic fracture of a panel.

5.1 Initial Profile Measurements

Figure 7 shows the measured profiles for all three panels. The data clearly show that the panels vary by up to ± 3 mm in shape, with the 1016-mm panel having the most severe initial imperfections. The initial profile data indicates that all panels were flattened along the length of the grip, indicating that the bolt-up process was successful in this regard. However, the data also show that, near the grip, the 1016-mm panel exhibited significant gradients normal to the grip line due to the bolt-up process.

Also, the data show that (a) the 305-mm panel has a saddle shape, (b) the 610-mm panel has a rounded shape with the same sign in curvature in both the X and Y directions, and (c) the 1016-mm panel has a significant local gradient near the centerline of the notch.

5.2 Panel Experiments and 3-D Displacement Measurements

Figure 8 presents the load-displacement data for all panel experiments. For each panel and all loads, the global 3-D system was used to determine the *panel displacement at one point* that was located on the panel just above the grip and near the specimen centerline throughout the loading process for comparison to available grip transducer measurements.

In the next three sections, global 3-D system measurements will be presented for each panel at three load levels that are representative of the deformation evolution process within each panel. In each case, the following terminology is employed to define the displacement components. The U displacement component is in the X direction and parallel to the notch length and/or perpendicular to loading direction. The V -displacement component is in the Y direction, which is perpendicular to the notch length and/or in the direction of the applied loading. The W -displacement is in the Z direction, which is perpendicular to the X and Y axes and along the through-thickness direction. Here $+W$ is toward the 3-D system (e.g., see Fig. 3).

In the last section, surface strain results around the termination hole, obtained using the local 3-D displacement data, will be presented for all three panels at the maximum loading.

5.2.1 Global 3-D displacement fields

Full-field, three-dimensional measurements for all panels are presented in this section. In the figures, the gray-scale levels for each component of displacement are the same for

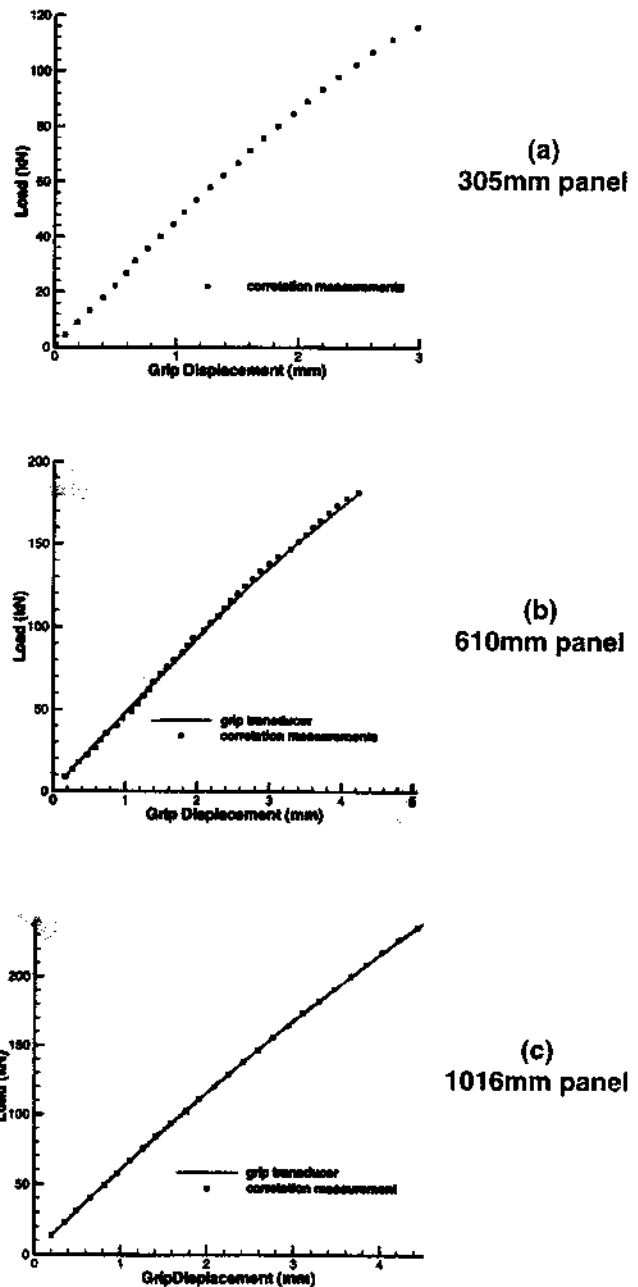


Fig. 8 Load-displacement data for all panels. Grip and direct panel data presented when measured.

all three panel sizes, however, the spacing of the contour lines, while consistent for any individual panel, was adjusted for each panel to best illustrate the underlying global field.

Global 3-D displacement fields for 305-mm panel. Full-field, three-dimensional displacement measurements for the 305-mm panel are presented in Fig. 9 for loads of 29, 58, and 116 kN, respectively. The U and V fields have contour lines indicating a change of 0.1 mm and the W -displacement field has 0.25-mm contours.

Global 3-D displacement fields for 610-mm panel. Full-field, three-dimensional displacement mea-

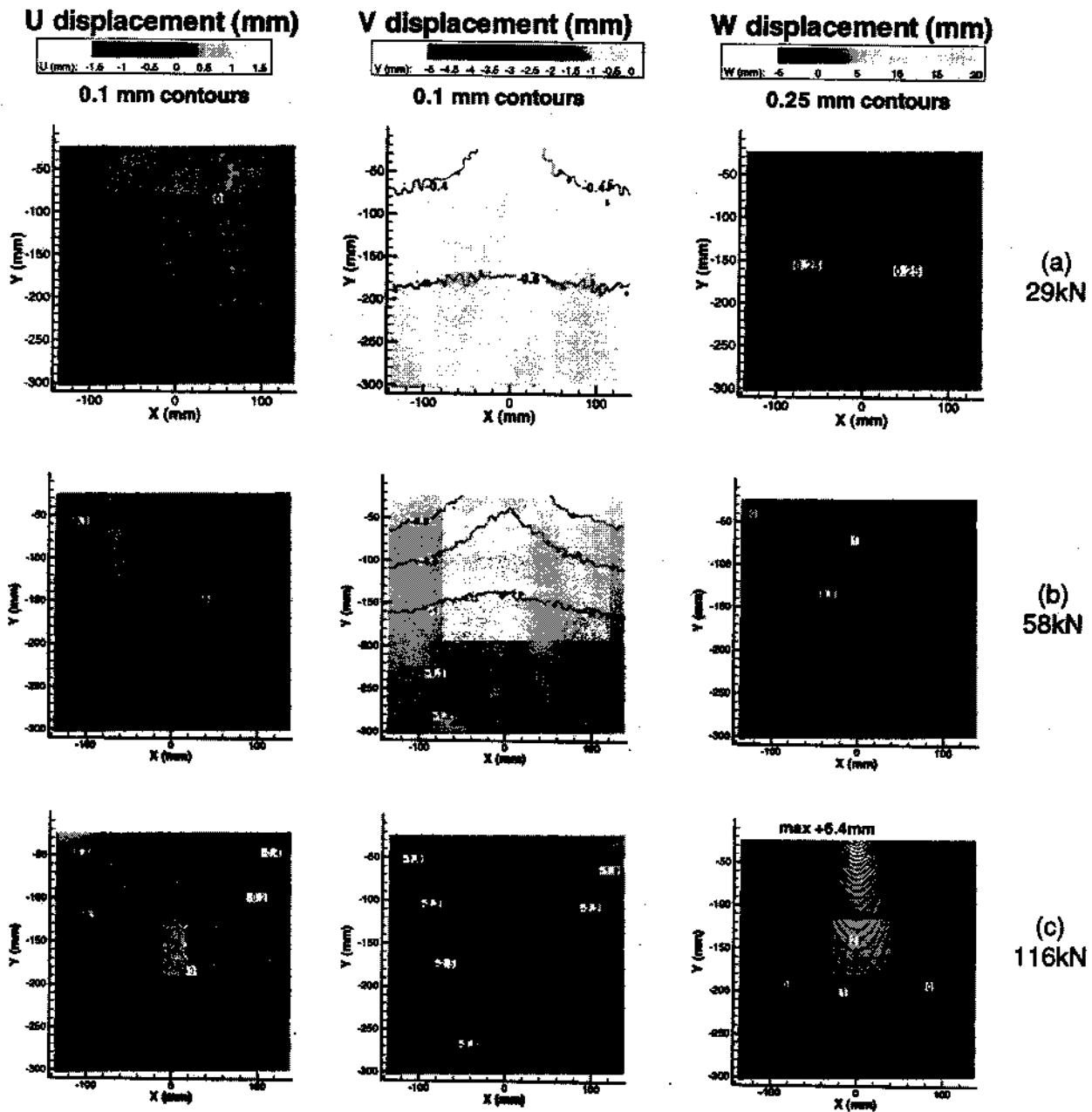


Fig. 9 3-D displacement data for 305-mm panel.

measurements for the 610-mm panel are presented in Fig. 10 for loads of 45, 89, and 178 kN, respectively. The U and V fields have contour lines indicating a change of 0.1 mm and the W -displacement field has 0.50-mm contours.

Global 3-D displacement fields for 1016-mm panel. Full-field, three-dimensional displacement measurements for the 1016-mm panel are presented in Fig. 11 for loads of 59, 120, and 236 kN, respectively. The U and V fields have contour lines indicating a change of 0.1 mm and the W -displacement field has 0.50-mm contours.

5.2.2 Local surface strain measurements for 305-, 610-, and 1016-mm panels

To convert the displacement measurements to strain fields, the following procedure was employed. First, a dense dis-

placement data cloud was measured (approximately 23,000 data points). Second, the data were transformed to a coordinate system aligned with the notch direction and with the X - Y plane aligned with the initial profile of the area. Third, points on the surface were selected for the strain measurements. Fourth, data within a 1.6-mm radius of a measurement point were selected. Fifth, a third-order surface was fitted to the data for each of the displacement fields. Sixth, differentiation of the surface fit was used to obtain the displacement gradients at the center of the area (the measurement point). Seventh, the strains were then calculated from the displacement gradients using a Lagrangian large strain formulation that includes the effects of local rotations. Finally, the procedure is repeated for the remaining measurement locations to obtain full-field strains in the region of interest.

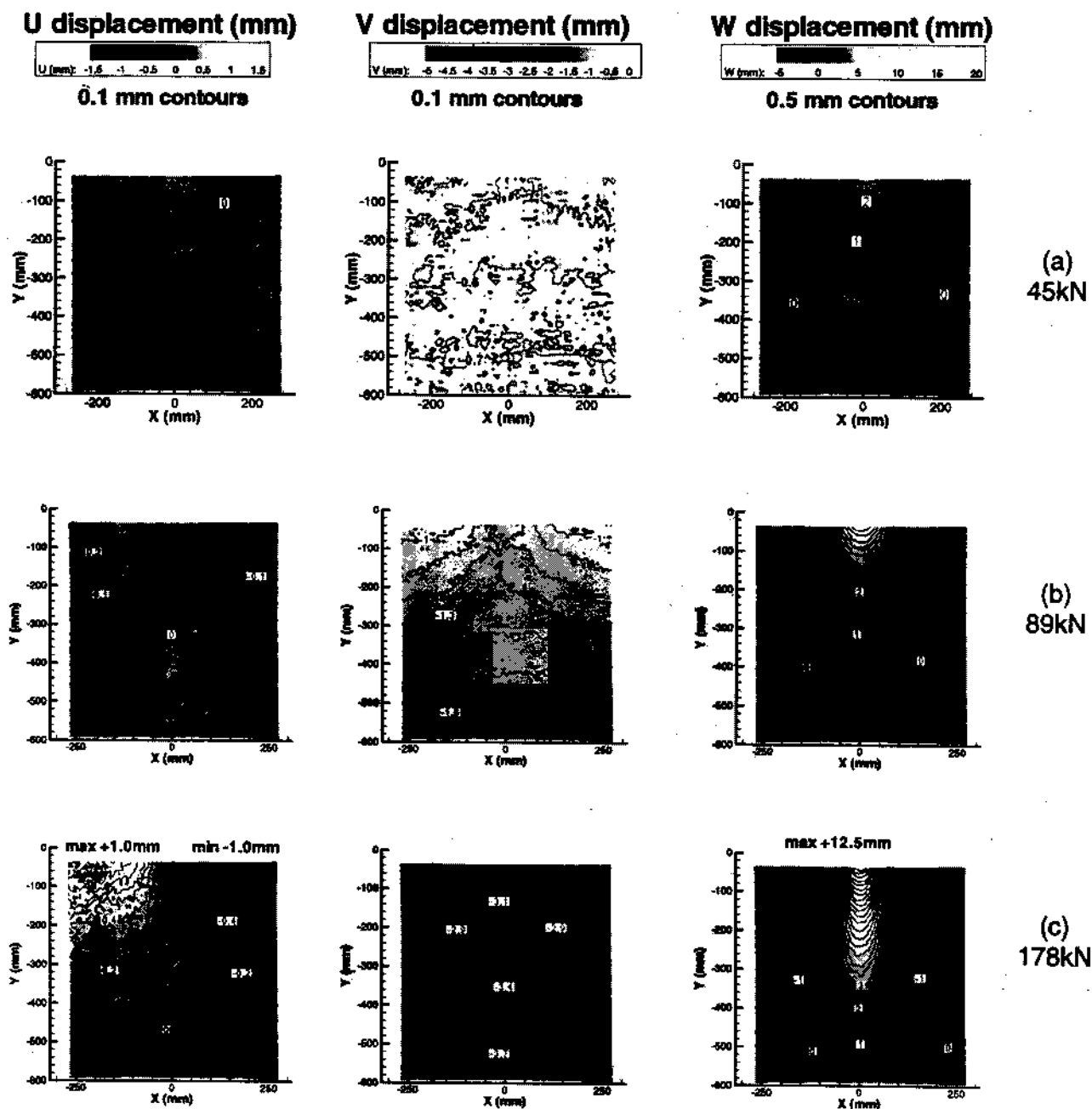


Fig. 10 3-D displacement data for 610-mm panel.

Figures 12 and 13 show the surface strains ϵ_{xx} , ϵ_{yy} , and ϵ_{xy} around the termination hole at the maximum load achieved by each of the three panels.

6 Discussion of Results

Figures 9–11 clearly shows that the global 3-D measurement system is capable of measuring true, three-dimensional structural deformations, both in regions having large out-of-plane displacements ($-3 \text{ mm} \leq W \leq 19 \text{ mm}$ in 1016-mm panel) and also in regions where the in-plane deformations are dominant. Furthermore, in regions of rapid change in one or more of the displacement components [e.g., see Figs. 9(c), 10(c), and 11(c)], the experimental data demonstrate that the measurement system is ca-

pable of resolving the large displacement gradients while simultaneously determining the remaining displacement component(s).

With regard to the large panel experiments, there are several points to note. First, as shown in Fig. 7, the 3-D measurements clearly show that each panel had an initial shape that deviated up to 3 mm from planarity, with local gradients occurring near the notch for the largest panel. Since such deviations may have a significant effect on analytical predictions, the global 3-D measurement of surface shape provides critical component geometry information for model development. It is worth noting that the measured deviations were simply not observable during visual examination of the as-installed panel, primarily due the fact

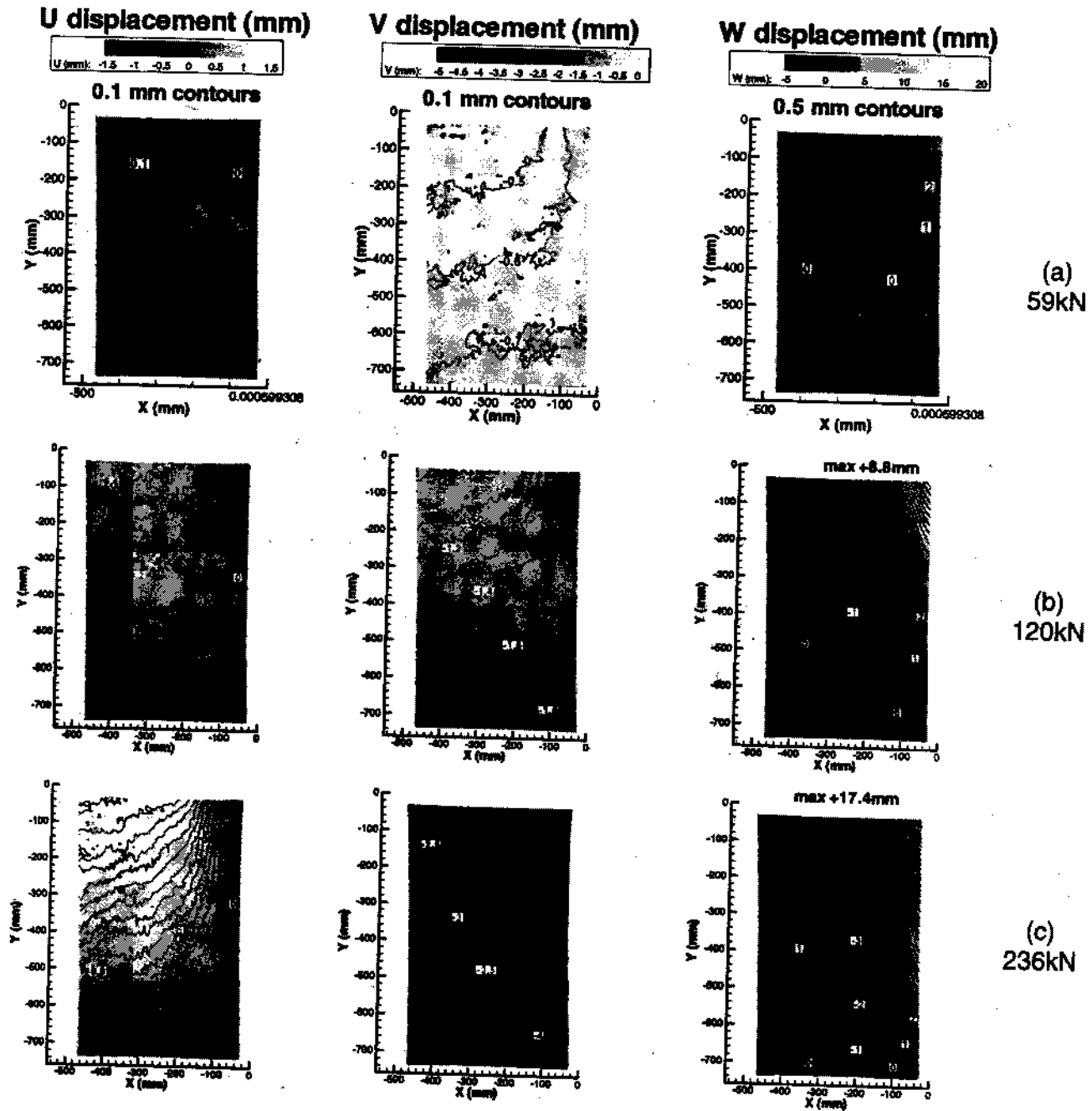


Fig. 11 3-D displacement data for 1016-mm panel.

that deviations are small compared to in-plane panel dimensions; $0.004 \leq d_{max}/w \leq 0.006$ for all the panels, where d_{max} is the maximum deviation from a best-fit plane.

Second, though not shown in detail, all panels initially flattened as the tensile loading increased. This can be most clearly seen in the W displacement of the 305-mm panel at 29 kN. The displacement field at this load is a reflection of the initial saddle shape of the panel. As the load increased past ~ 18 kN, all panels experienced a measurable and rapid rise in out-of-plane displacement along the notch, with the centerline notch displacement increasing monotonically with loading until final fracture occurred; the latter trend is observable in Figs. 9–11.

Third, as shown in Fig. 8, available grip transducer results are in close agreement with the centerline, single-point 3-D measurement of vertical displacement, indicating that the centerlines of both the 610- and 1016-mm panels were moving with the grips without measurable slippage. However, inspection of the full-field V -displacement data in the vicinity of the grip [see Fig. 11(b)] indicates that there is a clear gradient along the X direction in the V displacement from the centerline to the edge [see Fig. 10(b) for comparison]. Thus, though the centerline of the 1016-mm specimen is not slipping, the outer edge appears to have slipped by as much as 0.50 mm during the loading process.

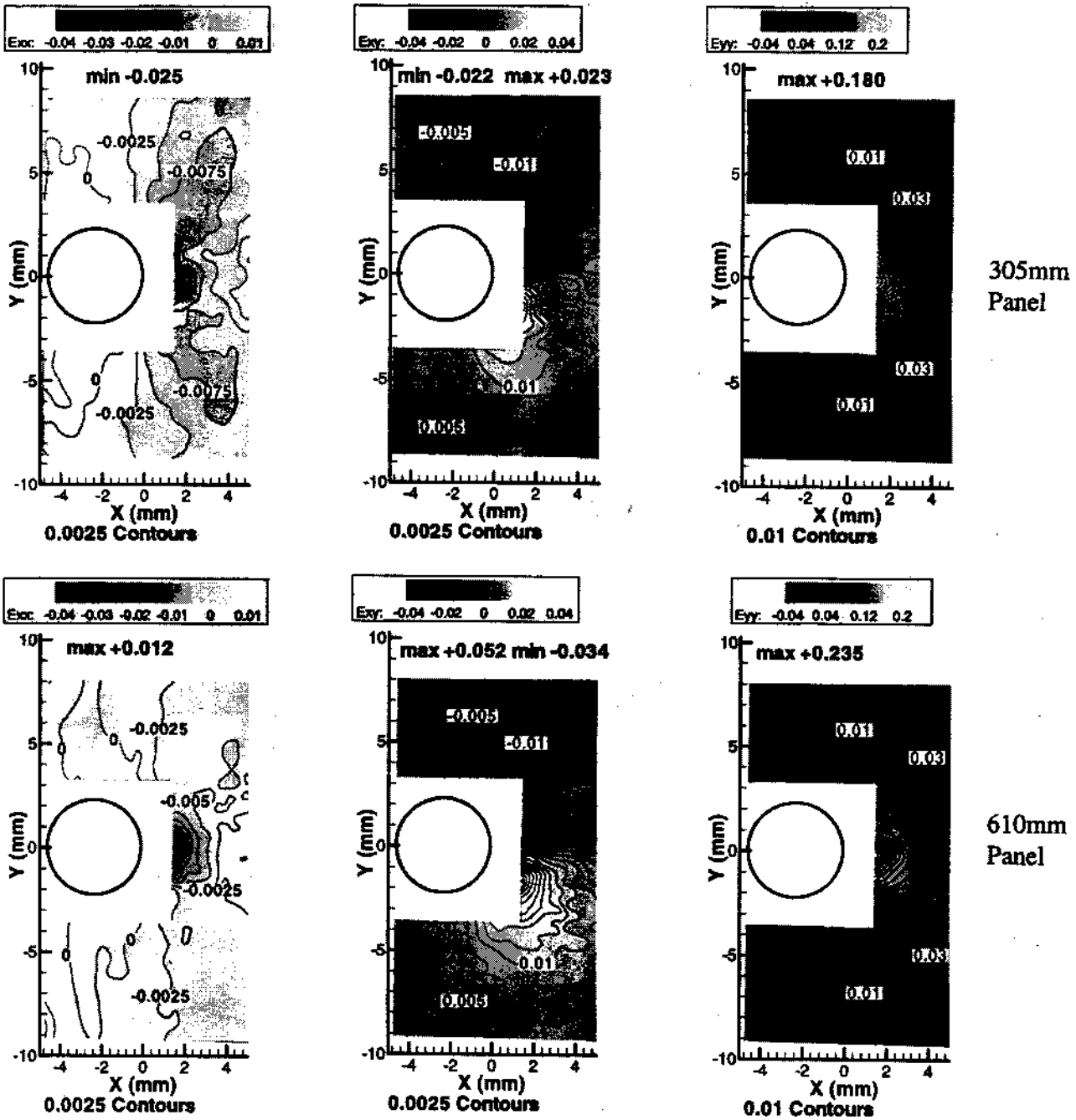


Fig. 12 Local strain field data at maximum loading for 305- and 610-mm panels.

Fourth, inspection of the W -displacement trends in Figs. 9–11 indicates that increasing the size of the specimen results in distinctly different surface deformations in the thin sheet. For example, the 305-mm panel had a maximum out-of-plane displacement at the specimen centerline, decreasing monotonically with distance along the X direction. In contrast, the 610-mm panel deformed so that it had an out-of-plane maximum at the centerline and minima at $X/w \cong \pm 0.50$ before increasing beyond the minima monotonically to the edge of the panel. Also, the 1016-mm panel deformed so that it had a maximum at the centerline, minima at $X/w \cong \pm 0.40$, and another maximum at $X/w \cong$

± 0.72 before decreasing slowly to the edge of the panel. Furthermore, the Y location of the first minima changes with panel geometry, from $Y/L = 0.31$ for the 610-mm panel to $Y/L = 0.45$ for the 1016-mm panel.

Fifth, the local strain fields shown in Figs. 12 and 13 are similar in appearance for all panels. The maximum measured tensile strain ranges from $\epsilon_{yy} \cong 15\%$ (305-mm panel) to $\epsilon_{yy} \cong 26\%$ (1016-mm panel). The tensile field has the appearance expected for plane stress conditions, with strains in excess of 2% extending horizontally several millimeters ahead of the termination hole. As expected, the

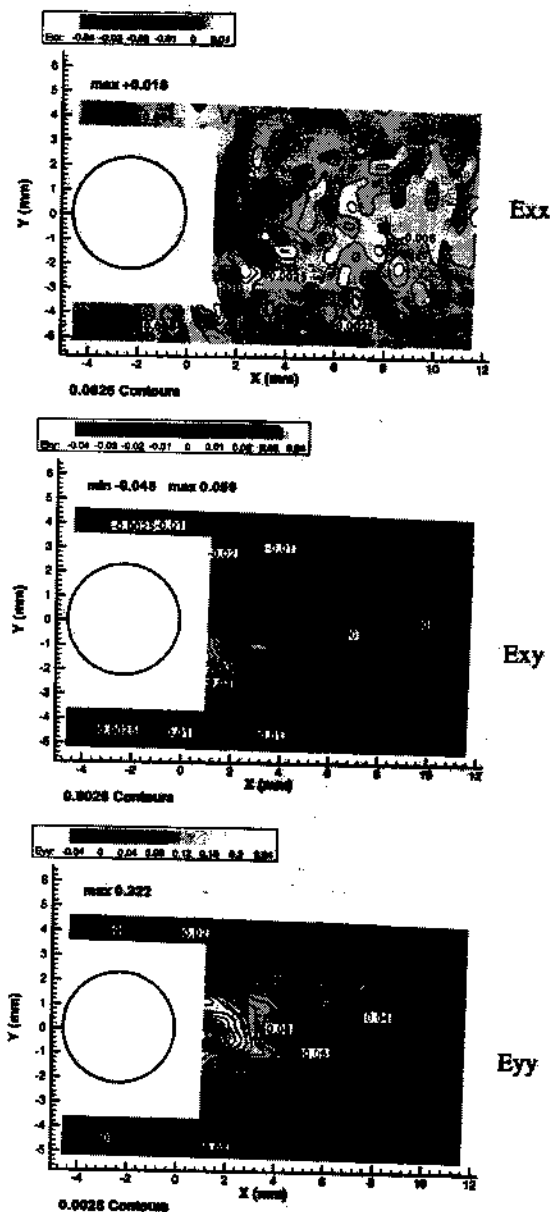


Fig. 13 Local strains at maximum load for 1016-mm panel.

values of ϵ_{xx} are negative ahead of the notch with a maximum measured value approaching -2% . The shear strain is antisymmetric about the X axis, extending along two lobes at ± 45 deg, with maximum and minimum values of $+3\%$ and -3% just ahead of the hole diameter. Similar to ϵ_{yy} , the estimated values for ϵ_{xy} decrease slowly along the lobes of maximum shear stress. Furthermore, for all specimens the regions of highest shear strain are circular in shape, a trend that is generally consistent with the expected plane stress conditions on the free surface.

7 Concluding Remarks

Results presented for both large measurement areas and small local regions near geometric discontinuities clearly demonstrate that both local and global deformations can be

determined simultaneously using independent optical arrangements that are designed for appropriate spatial and deformation resolution requirements.

The global load-displacement response shown in Fig. 7 is nearly linear for loadings up to approximately 90, 120, and 150 kN for the 305-, 610-, and 1016-mm panels, respectively. In each case, significant out-of-plane deformations and complex nonlinear behavior occurred well before any appreciable nonlinearity is observed in the global response. Since the highly localized, large deformations that occur near the notch will strongly influence the behavior of flaws in structural applications, the 3-D experimental measurements in these regions provide essential validation data for analytical tools.

Since 3-D stereovision measurement systems quantitatively determine the positions in space of small subregions, without regard for the complexity of the overall deformation field, these systems are ideally suited for complicated, highly nonlinear, structural response conditions.

Though the focus in this effort is on the acquisition of full-field measurements prior to crack extension to simplify the comparison to field-effect predictions, the 3-D digital image correlation (DIC) method is equally capable of making full-field measurements throughout the stable tearing process.^{13,14} Furthermore, provided that simultaneous stereo image pairs can be acquired, the 3-D DIC method is fully capable of measuring full-field, transient three-dimensional deformations during impact loading and dynamic fracture of nonplanar components.

Acknowledgments

The authors wish to thank former NASA Langley members Dr. James C. Newman, Jr., and Dr. David S. Dawicke, as well as current NASA Langley member Dr. Charles E. Harris, for their technical and financial support through both NAG-1-1489 and also a NASA GSRP Fellowship. The authors also wish to thank Mr. William Johnston of Lockheed-Martin for his help in conducting the panel tests. In addition, the support of NASA Headquarters and Dr. Julius Dasch through grant NCC5-174 is gratefully acknowledged.

References

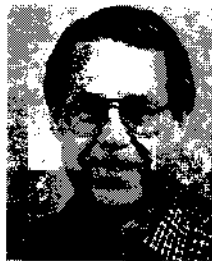
1. R. G. Forman, "Experimental program to determine effect of crack buckling and specimen dimensions on fracture toughness of thin materials," Technical Report AFFDL-TR-65-149 (Jan. 1966).
2. B. Alnroth, F. A. Brogan, and G. Stanley, "User's manual for STAGS," NASA CR 165670 (1978).
3. K. C. Koppenhoefer, A. S. Gullerud, C. Ruggieri, R. H. Dodds, and B. E. Healy, "WARP3D release 11.0 dynamic nonlinear analysis of solids using a preconditioned gradient software architecture," (Nov. 1998).
4. B. R. Seshadri, J. C. Newman, Jr., D. S. Dawicke, and R. D. Young, "Fracture analysis of the FAA/NASA wide stiffened panels," Second Joint NASA/FAA/DoD Conf. on Aging Aircraft (Jan. 1999).
5. J. G. Bakuckas, Jr., C. A. Bigelow, and P. W. Tan, "Full-scale Aircraft Structural Test and Evaluation Research Facility (FASTER)," 3rd Joint FAA/NASA/AFRL Conference on Aging Aircraft, Albuquerque, NM, 4B3A, 1-2 (1999).
6. J. H. Starnes, Jr. and C. R. Dawicke, "Effects of initial crack length on stable tearing and buckling of selected unstiffened aluminum shells subjected to internal pressure and axial compression," 1st Joint FAA/NASA/AFRL Conference on Aging Aircraft, 2, 1743-1765 (1997).
7. Z. L. Kahn-Jetter and T. C. Chu, "3-D displacement measurements using digital image correlation and photogrammetry techniques," *Exp. Mech.* 30(1), 10-16 (1990).
8. P. F. Luo, Y. J. Cha, and M. A. Sutton, "Application of stereo vision to 3-D deformation analyses in fracture experiments," *Opt. Eng.* 33(3), 981-990 (1994).

9. P. F. Luo, Y. J. Chao, M. A. Sutton, and W. H. Peters III, "Accurate measurement of three-dimensional deformations in deformable and rigid bodies using computer vision," *Exp. Mech.* 30(2), 123-132 (1993).
10. J. D. Helm, S. R. McNeill, and M. A. Sutton, "Improved three-dimensional image correlation for surface displacement measurement," *Opt. Eng.* 35(7), 1911-1920 (1996).
11. R. Y. Tsai, "An efficient and accurate camera calibration technique for 3-D machine vision," *Proc. IEEE Intl. Conf. Comp. Vision and Patt. Recog.*, 364-374 (1986).
12. J. Weng, P. Cohen, and M. Herniou, "Camera calibration with distortion models and accuracy evaluation," *IEEE Trans. Pattern Anal. Mach. Intell.* 14(10), 965-980 (1992).
13. J. D. Helm, M. A. Sutton, and M. L. Boone, "Characterizing crack growth in thin aluminum panels under tension-torsion loading using three-dimensional digital image correlation," *ASTM Spec. Tech. Publ.* 1323, 3-14 (2001).
14. M. A. Sutton, J. D. Helm, and M. L. Boone, "Experimental study of crack growth in thin sheet 2024-T3 aluminum under tension-torsion loadings," *Int. J. Fract.* 109, 285-301 (2001).
15. D. M. McGowan, D. R. Ambur, T. G. Hanna, and S. R. McNeill, "Evaluation of the compressive response of notched composite panels using full-field displacements," *J. Aircr.* 38(1), 122-129 (2001).
16. M. Born and E. Wolf, *Principles of Optics*, 3rd ed., pp. 203-233, Pergamon Press, Elmsford, NY (1964).
17. M. A. Sutton, S. R. McNeill, J. D. Helm, and H. S. Schreier, "Computer vision applied to shape and deformation measurement," in *Trends in Optical Non-Destructive Testing and Inspection*, P. K. Rastogi and D. Inaudi, Eds., 571-591, Elsevier (2000).
18. M. A. Sutton, S. R. McNeill, J. D. Helm, and Y. J. Chao, "Advances in 2-D and 3-D computer vision for shape and deformation measurements," in *Photomechanics*, P. K. Rastogi, Ed., *Topics in Applied Physics*, 77, 323-372, Springer Verlag, New York (2000).
19. M. A. Sutton, W. Zhao, S. R. McNeill, J. D. Helm, W. T. Riddell, and R. S. Piascik, "Local crack closure measurements: development and application of a measurement system using computer vision and a far-field microscope," *ASTM Spec. Tech. Publ.*, K. Smith and J. McDowell, Eds. 1343, 145-156 (1999).
20. T. C. Chu, W. F. Ranson, M. A. Sutton, and W. H. Peters III, "Application of digital image correlation techniques to experimental mechanics," *Exp. Mech.* 25(3), 232-245 (1985).
21. M. A. Sutton and Y. J. Chao, "Measurement of strains in a paper tensile specimen using computer vision and digital image correlation—part I: data acquisition and image analysis system," *J. Tech. Assoc. Paper Pulping Industry* 70(3), 173-175 (1988).
22. Y. J. Chao and M. A. Sutton, "Measurement of strains in a paper tensile specimen using computer vision and digital image correlation—part II: tensile specimen test," *J. Tech. Assoc. Paper Pulping Industry* 70(4), 153-156 (1988).
23. M. A. Sutton, T. L. Chae, J. L. Turner, and H. A. Bruck, "Development of a computer vision methodology for the analysis of surface deformations in magnified images," *ASTM Spec. Tech. Publ.* 1094, MICON-90, 109-132 (1990).



Jeffrey D. Helm received his BS and MS degrees in mechanical engineering from the University of South Carolina in 1992 and 1995, respectively. Dr. Helm completed his PhD in the Department of Mechanical Engineering at the University of South Carolina in 1999. Dr. Helm was the general manager of Correlated Solutions, a small company specializing in noncontacting measurement systems, before joining the faculty in the Department of Mechanical Engineering at Lafayette College in 2002. His research interests

include 2-D and 3-D computer vision based measurement systems, experimental fracture mechanics, and nondestructive evaluation techniques and applications.



Michael A. Sutton received his PhD in 1981 in theoretical and applied mechanics from the University of Illinois. Dr. Sutton joined the faculty in the Department of Mechanical Engineering at the University of South Carolina in 1982 and is now a Carolina distinguished professor. Prof. Sutton, a fellow and past president of the Society for Experimental Mechanics (SEM), has received numerous national and international honors for his contributions in the fields of experimental mechanics, computer vision, and fracture mechanics. Prof. Sutton has published more than 100 archival articles, co-authored four book chapters, and given numerous international presentations. Prof. Sutton is an active member in SEM, the American Society for Testing and Materials, and the American Society for Mechanical Engineering. He is director of both the South Carolina Center for NDE and Fracture Mechanics and also the USC Division of the S.C. NASA Space Grant Consortium. His current areas of research are experimental and analytical fracture mechanics, 2-D and 3-D computer vision, numerical methods, and mathematical modeling of problems.



Stephen R. McNeill received his BS from Georgia Institute of Technology in 1976, his MS from Auburn University in 1982, and his PhD from the University of South Carolina (USC) in 1986, all in mechanical engineering. Dr. McNeill joined the faculty in the Department of Mechanical Engineering at UCS upon completion of his doctorate and is currently an associate professor. He has been awarded USC's Michael J. Mungo teaching award in recognition of his teaching of undergraduates in mechanical engineering. The College of Engineering has recognized Dr. McNeill's teaching and service to the engineering profession by the awarding of their Samuel Litman Distinguished Professor Award in Engineering and the Joseph M. Biedenbach Distinguished Service Award. Dr. McNeill has been awarded several certificates of recognition from the National Aeronautics and Space Administration and USC for work in the area of digital image correlation. He has been awarded a patent for work in the area of radiographic image evaluation. He has other patent disclosures in the areas of automated lay-reversal detection systems, stain and crack-closure measurements systems, and full-field surface strain measurements systems. Prof. McNeill has published more than 40 archival articles, co-authored two book chapters, and given numerous presentations. Prof. McNeill is a member of the Society for Experimental Mechanics and the American Society of Mechanical Engineers (ASME). He has served as a faculty advisor for the USC student section of ASME and was named Region IV's faculty advisor of the year for his work with students. He has also served as president of the Midland's section of ASME. His current areas of research are in 2-D and 3-D digital image correlation with current emphases on ultra-high-speed image acquisition. He is also involved with characterization of impact damage in armor materials.